The Cryosphere
Discussions
Open Access
EGU

1   Spatiotemporal variation of snow depth in the Northern Hemisphere from 1992 to 2016

3   Xiongxin Xiao[1, 2], Tingjun Zhang[1, 4], Xinyue Zhong[3], Xiaodong Li[1], Yuxing Li[1]

4   [1]Key Laboratory of Western China's Environmental Systems (Ministry of Education), College of Earth
5   and Environment Sciences, Lanzhou University, Lanzhou 730000, China
6   [2]School of Remote Sensing and Information Engineering, Wuhan University, Wuhan 430079, China
7   [3]Key Laboratory of Remote Sensing of Gansu Province, Cold and Arid Regions Environmental and
8   Engineering Research Institute, Chinese Academy of Sciences, Lanzhou 730000, China
9   [4]University Corporation for Polar Research, Beijing 100875, China.

10   *Correspondence to*: Tingjun Zhang (tjzhang@lzu.edu.cn)

11   **Abstract:** Snow cover is an effective best indicator of climate change due to its effect on regional and

12   global surface energy, water balance, hydrology, climate, and ecosystem function. We developed a long

13   term Northern Hemisphere daily snow depth and snow water equivalent product (NHSnow) by the

14   application of the support vector regression (SVR) snow depth retrieval algorithm to historical passive

15   microwave sensors from 1992 to 2016. The accuracies of the snow depth product were evaluated

16   against observed snow depth at meteorological stations along with the other two snow cover products

17   (GlobSnow and ERA-Interim/Land) across the Northern Hemisphere. The evaluation results showed

18   that NHSnow performs generally well with relatively high accuracy. Further analysis were performed

19   across the Northern Hemisphere during 1992-2016, which used snow depth, total snow water

20   equivalent (snow mass) and, snow cover days as indexes. Analysis showed the total snow water

21   equivalent has a significant declining trends (~5794 km^3 yr.$^{-1}$, 12.5% reduction). Although spatial

22   variation pattern of snow depth and snow cover days exhibited slight regional differences, it generally

23   reveals a decreasing trend over most of the Northern Hemisphere. Our work provides evidence that

24   rapid changes in snow depth and total snow water equivalent are occurring beginning at the turn of the

25   21st century with dramatic, surface-based warming.

26   **1. Introduction**

27   Seasonal snow cover is an important component of the climate system and global water cycle that

28   stores large amounts of freshwater and play major impacts on the surface energy budget, climatology

29   and water management (Immerzeel et al., 2010;Zhang, 2005;Robinson and Frei, 2000;Tedesco et al.,

1   2014). On account of the high albedo and low heat conductivity properties of snow, snow cover may

2   directly modulate the land surface energy balance (Flanner et al., 2011), influence on soil thermal

3   regime (Zhang et al., 1996;Zhang, 2005), and indirectly affect atmospheric circulation (Cohen et al.,

4   2012;Zhang et al., 2004;Li et al., 2018). Most jurisdictions in the Northern Hemisphere rely on natural

5   water storage provided by snowpack (Diffenbaugh et al., 2013;Barnett et al., 2005), supplying water for

6   domestic and industrial use (Sturm, 2015;Qin et al., 2006). Accurate estimation of and reliable

7   information on snow cover spatial and temporal change at regional and global scales is very critical for

8   climate change monitoring, model evaluation and water source management (Brown and Frei,

9   2007;Flanner et al., 2011).

10   Snow depth (SD) is most commonly measured using in situ observations. Given the sparseness of

11   measurements, it is not possible to fully capture spatial variability of snow cover. Although the in situ

12   observation method is accurate, it is unrealistic in mountain regions and low population zones because

13   it is labor, material and financial resource intensive. Remote sensing is the most effective and powerful

14   way of obtaining information of snow cover over larger areas (Foster et al., 2011). Optical remote

15   sensing is capable of observing large areas of snow; however, it is unable to observe the Earth's surface

16   under cloudy conditions (Foster et al., 2011;Che et al., 2016;Dai et al., 2017). However, microwave

17   remote sensing has this potential and is an attractive alternative to optical remote sensing under all

18   weather conditions and round the clock. It can also be used to estimate SD and snow water equivalent

19   (SWE) due to the interaction with snowpack by providing dual polarization data at different

20   frequencies (Chang et al., 1987;Che et al., 2008;Takala et al., 2011).

21   Snow cover products derived from passive microwave (PM) data have been widely applied to

22   investigate regional and global climate change, and validate hydrological and climate models (Brown et

23   al., 2010;Brown and Robinson, 2011;Dai et al., 2017). Progress in satellite data acquisition, as well as

24   SD/SWE retrieval algorithm development, have led to a global improvement in snow monitoring (Qin

25   et al., 2006;Snauffer et al., 2016). The PM brightness temperature of the SMMR (Scanning

26   Multichannel Microwave Radiometer), SSM/I (Special Sensor Microwave Imager), AMSR-E

27   (Advanced Microwave Scanning Radiometer for Earth Observing System), AMSR2 (Advanced

28   Microwave Scanning Radiometer 2 on the Global Change Observation Mission – Water), SSMIS

29   (Special Sensor Microwave Imager), SSM/I (Special Sensor Microwave Imager Sounder) and,

30   FY-3B/C (Fengyun-3 satellite B/C) are available and several algorithms have been developed to

1   estimate SD and SWE using PM brightness temperature data (Chang et al., 1987;Dai et al., 2012;Xiao

2   et al., 2018;Pulliainen, 2006;Takala et al., 2011;Che et al., 2008;Foster et al., 1997).

3   Most retrieval algorithms operate on the principle that the difference in brightness temperature

4   between 18 and 37 GHz reflects the quantity of SD and SWE (Chang et al., 1987). Over and

5   underestimated trends are prevalent in these linear SD and SWE retrieval algorithms (Gan et al., 2013)

6   for which there are two possible and reasonable explanations. One is that vegetation overlaying snow

7   attenuates its microwave scatter signal and results in underestimating SD and SWE from PM data (Che

8   et al., 2016;Vander Jagt et al., 2013). To reduce the effect of tree canopy, a forest fraction was

9   introduced into retrieval algorithm developed to estimate SD and SWE (Foster et al., 1997;Che et al.,

10   2008), or the retrieval algorithm was constructed based on particular land cover types (Goïta et al.,

11   2003;Che et al., 2016;Derksen et al., 2005;Foster et al., 2009). The other explanation is that the

12   relationship between snow properties (SD or SWE) and the PM brightness temperature is non-linear.

13   Newer approaches (e.g. artificial neural networks, support vector regression, decision tree) have

14   emerged using data-mining and have been explored to retrieve SD and SWE that are intended to

15   replace traditional linear methods (Gharaei-Manesh et al., 2016;Tedesco et al., 2004;Liang et al.,

16   2015;Forman et al., 2013;Xue and Forman, 2015). However, there are remain some limitations for

17   these retrieval algorithms due to the diversity of land cover types and the spatiotemporal heterogeneity

18   of snow physical properties.

19   Numerous studies have reported the changes in snow cover extent (SCE) at regional and

20   hemispheric scales (Rupp et al., 2013;Dai et al., 2017;Derksen and Brown, 2012;Brown and Robinson,

21   2011;Huang et al., 2016). Huang et al. (2017) repored the impact of climate and elevaion on snow

22   cover varition in Tibetan Plateau, including SWE, snow cover area and, snow cover days. Hori et al.

23   (2017) developed a 38-year Northern Hemisphere daily snow cover extent product and analyzed

24   seasonal Northern Heimsphere snow cover extent variation trends. In this study, SD was selected as

25   basis for analyzing spatiotemporal change of snow cover. SD provides an additional dimension to snow

26   cover characteristics. Barrett et al. (2015) explored intra-seasonal variability in springtime Northern

27   Hemisphere daily SD change by the phase of the Madden–Julian oscillation. Wegmann et al. (2017)

28   compared four long-term reanalysis datasets with Russian SD observation data. However, this study

29   only focused on snowfall season (October and November) and snowmelt season (April). SD change

30   trends have also been analyzed at regional scales (Ye et al., 1998;Dyer and Mote, 2006). Several studies

The Cryosphere

Discussions

Open Access

1   quantified the spatial and temporal changes consistency of SWE or snow mass derived from satellite

2   data (Mudryk et al., 2015) but these studies have focused on the limited dimension of snow cover

3   variation. Dyer and Mote used a gridded dataset to study regional and temporal variability of SD trends

4   across North America from 1960-2000 (Dyer and Mote, 2006) and the characteristic of seasonal snow

5   extent and snow mass in South America form 1979 to 2006 was descripted and reported (Foster et al.,

6   2009).

7   There are, however, very limited data (station data, satellite data or otherwise) that can provide

8   both SD and SWE on a hemispheric scale. This paper describes the approach to develop a consistent

9   25-year of daily SD and SWE of Northern Hemisphere utilized multi-source data. The primary

10 objective of this study is to develop 25 years (1992-2016) hemispherical SD and SWE product

11 (hereafter referred to as the NHSnow) with a 25 km spatial resolution using SVR SD retrieval

12 algorithm. This paper will address the following questions: 1) How consistent are NHSnow and other

13 sourced snow cover datasets with the in situ SD observation? 2) What is the spatiotemporal variability

14 of snow cover in the Northern Hemisphere from 1992-2016? Meanwhile, it is extremely challenging to

15 make extensive quantitative validation of SD and SWE estimates.

16   This paper is organized in five sections, as follows. Section 2 describes the data sets used in this

17 study. The methods of data preprocessing and snow cover products generation were provided in

18 Section 3. Next, we describe NHSnow validation against in-situ snow observation record, exhibit the

19 variability of snow cover in the Northern Hemisphere and discuss the potential effect factors for the

20 variation results utilized NHSnow data (Section 4). Finally, section 5 summarizes the work of this

21 paper.

22 **2 Datasets**

23 **2.1 Passive microwave data**

24   Because cloud often appear in the snow cover region or condition, during the winter season often

25 conceals snowfall possibility, here is particularly advantageous using passive microwave remote

26 sensing. SSM/I and SSMIS is PM radiometer onboard United States Defense Meteorological Satellites

27 Program (DMSP) satellite (available from the National Snow and Ice Data Center,

28 http://nsidc.org/data/NSIDC-0032). The SSM/I (F11 and F13) dataset from this platform, as well as

1   SSMIS (F17), present with the equal-area scale earth grid (EASE-Grid) format and 25 km spatial

2   resolution (Brodzik and Knowles, 2002;Armstrong, 2008;Wentz, 2013;Armstrong and Brodzik, 1995)

3   (Table 1). The snow cover area and SD derived from SSM/I (F11) and SSM/I (F13) data have high

4   consistency rendering the calibration between these two sensors for snow cover area and SD

5   unnecessary (Dai et al., 2015). To minimize the melt-water effect to some extent, which can change the

6   microwave emissivity of snow, only descending orbit (nighttime) passive microwave data were used

7   (Foster et al., 2009).

8   **2.2 Ground-based data**

9   Ground SD observation are used to construct and verify the SD retrieval model in this study from

10   two sources of daily SD observation. The first is the Global Surface Summary of the Day (GSOD)

11   dataset   provided   by   National   Oceanic   and   Atmospheric   Administration   (NOAA)

12   (https://data.noaa.gov/dataset/dataset/global-surface-summary-of-the-day-gsod). This online dataset,

13   which began in 1929, is derived from the Integrated Surface Hourly (ISH) dataset (Xu et al., 2016).

14   There are fourteen daily elements in GSOD dataset, including SD measured at 0.1 inch. The missing of

15   SD or reported 0 on the day would be marked 999.9. Data at approximately 30000 meteorological

16   stations were recorded of which 9000 typically are valid. In our study period and area, more than 17

17   000 meteorological station were selected with records from 1991 and a location far from large water

18   bodies.

19   To supplement data from stations that were not reporting during the study periods, ground-based

20   measurements of daily SD were gathered from an additional 635 Chinese meteorological stations

21   available at the National Meteorological Information of China Meteorological Administration (Xiao et

22   al., 2018;Zhong, 2014). These daily SD records begun in 1957 include SD (unit, cm), observation time,

23   and geographical location information available (http://data.cma.cn/en).

24   **2.3 Topographic and land cover data**

25   We also used topography as an auxiliary information to estimate SD (Xiao et al., 2018). Elevation

26   was   available   from   ETOPO1   at   a   resolution   of   1   arc-minute   (Amante, 2009)   available   at

27   (http://www.ngdc.noaa.gov/mgg/global/). To match the resolution of the PM brightness temperature

28   data with 25 km spatial resolution, we resampled the ETOPO1 to 25 km resolution (Fig. 1).

1   To increase the accuracy of SD estimates for different land cover types, we both used MODIS land

2   cover (MCD12Q1 V051) from 2001 to 2013 (Friedl and Sulla-Menashe, 2011;Friedl et al., 2010) and

3   Advanced Very High Resolution Radiometer (AVHRR) Global Land Cover classification generated by

4   the University of Maryland Department of Geography. The MCD12Q1 International

5   Geosphere-Biosphere Program (IGBP) classification scheme divides land surface into 17 types, which

6   were reclassified into five classes according to Xiao et al (2018) study.

7   AVHRR imagery was acquired between 1981-1994 from the NOAA-15 satellite (Hansen et al.,

8   2000) and were categorized into fourteen land cover classes at 1 km resolution. These data allowed us

9   to adjust the proposed snow-depth retrieval algorithm by reclassifying the fourteen native land cover

10   classes into five classes (water, forest, shrub, prairie and, bare-land) at 25 km spatial resolution (Table

11   A.). MCD12Q1 is available at site https://earthdata.nasa.gov/, while AVHRR land cover data is

12   available from http://www.landcover.org/data/landcover/.

13   **2.4 Satellite snow cover datasets**

14   Two kinds of snow cover datasets were utilized based on two criteria: covering the Northern

15   Hemisphere and long-term availability. We selected GlobSnow and ERA-Interim/Land which are

16   widely used in global and regional climate change studies (Snauffer et al., 2016;Hancock et al.,

17   2013;Mudryk et al., 2015). These datasets were used to compare with the NHSnow SD product.

18   In November 2013, the European Space Agency (ESA) released the GlobSnow Version 2.0 SWE

19   and Snow Extent (SE) data for the Northern Hemisphere (Takala et al., 2011;Pulliainen, 2006). These

20   data include all non-mountainous areas in the Northern Hemisphere and are available online

21   (http://www.globsnow.info/). Processing includes data assimilation based on combining satellite PM

22   remote sensing data (SMMR, SSM/I and SSMIS), spanning December 1979 to May 2016, with

23   ground-based observation data in a data assimilation scheme to derive SWE. GlobSnow Version 2.0

24   (hereinafter referred as GlobSnow) provides three kinds of temporal aggregation level products with

25   25 km spatial resolution: daily, weekly and monthly. This dataset covers all land surface areas in a

26   band between 35° N ~ 85° N excluding mountainous regions, glaciers and Greenland. To convert

27   between SD and SWE using GlobSnow, the snow density is held constant at 0.24 g/cm^3 (Sturm et al.,

28   2010;Hancock et al., 2013;Che et al., 2016).

29   ERA-Interim/Land (Balsamo et al., 2015) is a global land-surface reanalysis product with data

1   from January 1979 to December 2010 based on ERA-Interim meteorological forcing. It is produced by

2   a land-surface model simulation using the Hydrology Tiled ECMWF Scheme of Surface Exchange

3   over Land (HTESSEL), with meteorological forcing from ERA-Interim. Dutra et al. (2010) described

4   the snow scheme and demonstrated the verification using field experiments. "SD", which actually is

5   SWE, is one of the thirteen parameters provided. We should convert SWE to SD using the associated

6   snow density data. These two datasets are available online

7   (http://apps.ecmwf.int/datasets/data/interim-land/type=an/). To maximum the proximity to the

8   descending orbit time of passive microwave sensor, the data with analysis type at 6 o'clock were used

9   in this study, and the spatial resolution of these data is 0.125 degree.

10   **2.5 Snow classification data**

11   In order to accurately estimate SWE, snow classification data were used to convert SD into SWE.

12   Global Seasonal Snow Classification System was defined by Sturm et al. (1995) based on snow

13   physical properties (SD, thermal conductivity, snow density snow layers, degree of wetting, etc.), and

14   seasonal snow cover. Snow cover were categorized into six snow classes (tundra, taiga, alpine,

15   maritime, prairie, and ephemeral) plus water and ice fields (Figure 2). Snow classification data can be

16   accessed from the National Center for Atmospheric Research (NCAR)/Earth Observing Laboratory

17   (EOL) (https://data.eol.ucar.edu/dataset/6808). The snow classification dataset was developed and

18   tested for the Northern Hemisphere at 0.5-degree spatial resolution(Sturm et al., 1995).

19   **3 Methods**

20   **3.1 Theoretical basis**

21   Snow distribution is affected by various factors, but not limited to, vegetation (Che et al.,

22   2016;Vander Jagt et al., 2013), soil and air temperature (Forman and Reichle, 2015;Grippa et al.,

23   2004;Dai et al., 2017), topography and wind (Smith and Bookhagen, 2016). The snow retrieval process

24   uses DS and other parameters (A, T, G, L, D ...) to yield snow parameters (e.g. SD, Eq. 1) (Xiao et al.,

25   2018).

$$[S] = g\ (A,\ T,\ G,\ L,\ DS,\ D\ ...) + \varepsilon \qquad\qquad (1)$$

26   where g (·) denotes the retrieval function. DS is the digital signal from remote sensing sensor (PM,

1   active microwave, visible spectral remote sensing etc.), A is the atmosphere (wind speed, air

2   temperature, humidity, precipitation etc.), T is the topography (latitude, longitude, elevation, terrain

3   slope, aspect etc.), L is the location (latitude, longitude), G is the ground (ground surface temperature,

4   vegetation type etc.), S is the snow properties (snow grain size, density, reflectance, SD, SWE etc.), D

5   is the day of year and ε is the residual error or uncertainty that describes the relationship between

6   sensor signal and measured snow properties.

7   The SVR SD retrieval algorithm also follows the snow retrieval process (Eq. 1). We utilized ten

8   parameters were as input parameters, including PM brightness temperature (19 GHz, 37 GHz, 85 GHz,

9   or 91 GHz) with vertical and horizontal polarizations, geophysical location (latitude and longitude),

10   elevation and, the measured SD. The output parameter is the estimated SD. Apart from above factors,

11   the SVR SD retrieval algorithm also considers other influence factors, including wet snow, land cover

12   types and day of year (Xiao et al., 2018) to improve the accuracy of estimated SD. Day of year have

13   been converted into three snow cover stages, which mean indirectly considering snow properties

14   evolution.

15   **3.2 Processing flow overview**

16   The SVR SD retrieval algorithm first proposed by Xiao et al. (2018), which indirectly considers

17   seasonal variation and vegetation influence in the evolution of snow properties, was used to estimate

18   SD. In Eurasia, it was found that the SVR SD retrieval algorithm performs much superior with reduced

19   uncertainties compared based upon the correlation coefficient (R), mean absolute error (MAE), and

20   root mean squared error in Xiao et al. (2018) study. It should be noted that this study used daily

21   observation in the Northern Hemisphere with exception of July and August. Here, we provide more

22   detailed but different descriptions for the SVR SD retrieval algorithm in several steps (Fig. 3). The

23   detailed descriptions of the other steps can refer to the Xiao et al paper (Xiao et al., 2018) not repeated

24   here.

25   Step 3. Due to our study period pre-dates MODIS data, we used AVHRR land cover as suppliment

26   data. MODIS and AVHRR land cover were reclassified into four classes (forest, prairie, shrub and

27   bare-land) which were bases of construting SD retrieval sub-model. Table A (in appendix) describes the

28   reclassification scheme of AVHRR land cover is described. MODIS land cover reclassification schemes

29   were documented in Xiao et al. (2018). Because of the relative stability of land cover change, MODIS

1   land cover in 2013 was used for each year during 2013–2016. Similarly, MODIS land cover in 2001

2   was used in each year during 1998–2001, and AVHRR land cover data were used for 6 years

3   (1992–1997).

4   Step 6.1 Construction of a subcontinental model. It needs to be stressed that the snow properties in

5   the Eurasia (EU) and North America (NA) exhibit noticed discrepancy especially in snow density.

6   (Zhong et al., 2014;Bilello, 1984). One study pointed out that mean snow density in the former Soviet

7   Union (0.21 ~ 0.31 g/cm^3) was lower than the data from NA (0.24 ~ 0.31 g/cm^3) (Bilello, 1984), and

8   also Zhong et al. (2014) explained the possible reasons which resulting in the diversity of snow density

9   in EU and NA. Based on this, we separately constructed the SD retrieval models for EU and NA.

10   Step 6.2 Training dataset selection is the process of removing redundant features from spatial data.

11 The accuracy of estimated SD primarily depends on training data quality, which also demonstrate the

12 significance of the selection rule of training samples (Xiao et al., 2018). Inputting more data than

13 needed in the training dataset to train SD retrieval model, may lead to overfitting and an estimated SD

14 with high error. In this study, we collected an extremely large number of daily SD records over 25 years,

15 necessitating a optimized selection rule to avoid data information redundancy.

16   The selection rule proposed in previous research (Xiao et al., 2018) was modified and then it was

17 divided into two steps in here. Firstly, the numbers of sample in the three layers, layer1 (0≤SD<50),

18 layer2 (50≤SD<100) and layer3 (SD≥100), should be concretely quantified. To avoid an inflated

19 training sample in layer2 and layer3, we set a threshold (3 000) determined by several tests (not shown).

20 A threshold (12000) for layer1 was adopted following Xiao et al. (2018). Table 2 described the section

21 of training sample for each layer in detail. After that, the quality of training sample in each layers

22 determined by stratified random sampling is the second step. Stratification was performed in 1 cm SD

23 intervals. Note that, all the selecton operations in here were randomly performed.

24   Step 7. Through above steps, the daily estimated SD data in the Northern Hemisphere from

25 January 1992 to December 2016 (excluding July and August) were obtained. Owning to the nature of

26 radiometer observations, NHSnow products are only reliable in areas with seasonal dry snow cover.

27 Areas with sporadic wet or thin snow are not reliably detected and areas marked as snow-free may

28 include areas with wet snow. If one pixel is detected as snow cover by the detection decision tree

29 (Grody and Basist, 1996), but is likely to be shallow or medium-to-deep snow with an estimated value

30 of equal or less than 1 cm, the SD value is set as 5 cm (Che et al., 2016;Wang et al., 2008) (Fig. 4.).

1   Step 8. In this study, Greenland and Iceland are excluded from the generation and analysis of

2   NHSnow (NH_SD, NH_SWE) products due to their complex coastal topography and the difficulty in

3   discriminating snow from ice (Fig. 4) (Brown et al., 2010). Missing data and zero-data gaps occur in

4   the process of generating daily SD gridded products. Therefore, the following filters were applied.

5   Daily estimated SD was averaged with a sliding 7-day window to reduce noise and compensate for

6   missing data in the daily time series. For example, the SD estimate for 4 January is an average of the

7   assimilated scheme output for 1 to 7 January (Takala et al., 2011;Che et al., 2016). When finished, the

8   sliding SD method generated daily SD products for the entire Northern Hemisphere (NH_SD; Fig. 4).

9   **3.3 Estimation of SWE**

10   SWE contains more useful information for hydrologists than SD because it represents the amount

11   of liquid water in the snowpack available to the ecosystem as the snow melts. One way to estimate

12   SWE uses SD and snow density (ρ) as described in Eq. 2. Northern Hemisphere SWE products were

13   generated in this study using snow density that converts SD to SWE. (Eq. 2, Fig. 3 and 4, Step 9).

$$\text{SWE}(mm) = \text{SD}(cm) \times \rho(g/cm^3) \times 10 \qquad (2)$$

14   At present, the primary problem is to obtain relatively accurate snow density. In this study,

15   dynamical calculation methods were adopted to estimate snow density. Two methods are usually used

16   to convert SD to SWE. The first uses a fixed value, 0.24 g/cm^3 (or other value), without spatiotemporal

17   variation (Che et al., 2016;Takala et al., 2011). The second uses a temporally static by spatially variable

18   mask of snow density to estimate SWE and are used to generate current AMSR-E SWE products

19   (Tedesco and Narvekar, 2010). Since the snowpack are usually rather unstable, it is awfully

20   unreasonable to set the snow density in the whole snow season to a constant. Observations show that

21   snow density does evolve and tends to increase (decrease) throughout the snow season (from

22   September to June) (Dai et al., 2012;Sturm et al., 1995). Here, daily snow density is obtained following

23   Sturm et al.(2010) (Eq. 3).They used daily SD, day of the year (DOY), and the snow climate class (SC)

24   to produce snowpack bulk density estimates. In this method, knowledge of SC is used to capture field

25   environment variables (air temperature, initial density) that have a considerable effect on snow density

26   evolution.

$$\rho(\text{SD,DOY,SC}) = (\rho_{max} - \rho_0)[1 - exp(- k_1 \times SD - k_2 \times DOY)] + \rho_0 \qquad (3)$$

27   where ρ_{max} is the maximum density, ρ_0 is the initial density, k_1 and k_2 are densification

1   parameters for SD and DOY, respectively. k_1, k_2, ρ_{max}, ρ_0 vary with SC (Table 3). For operational

2   purposes in our work, DOY extend to 1 September each year (Matthew Sturm, personal

3   communication, 2018) running from −122 (1 September) to 181 (30 June). Sturm et al. (2010) didn't

4   compute snow density for the SC as ephemeral snow despite its presence in the Northern Hemisphere.

5   According to Zhong et al. (2014) study, the snow density of ephemeral is set to an fixed value, 0.25

6   g/cm^3. Finally, daily snow density is simulated by the Eq. 3 in the Northern Hemisphere during the

7   1992−2016 period.

8   **4 Results and Discussion**

9   **4.1 Snow depth**

10   **4.1.1 Validation of snow depth**

11   Here to give insight into relative performance of SD products, we compared three sources of snow

12   cover product (NHSnow, GlobSnow, and ERA-Interim/Land) with ground SD observations (Fig. 5-7)

13   using three indices bias, mean absolute error (MAE) and root mean square error (RMSE).The common

14   period (1992 - 2010) daily SD of three products (Section 2.4) were collected as validation data. This

15   validation work primarily focus on snow cover stabilization stage (December to February). Since the

16   snow density change slowly over a smaller range in snow cover stabilization stage (Xiao et al., 2018),

17   using a constant value (0.24 g/cm^3) for GlobSnow could introduce relative little error (Section 3.3).

18   Subject to the unavailability of SWE station observations, the evaluation of SWE can't be carried out.

19   The relatively little bias (blue and green dots) between the estimated SD from three products

20   against measured SD is located in mid and low latitude regions (< 60 °N) for these three snow depth

21   datasets (NHSnow, GlobSnow, and ERA-Interim/Land; Fig. 5). However, a large bias was found in the

22   polar region and along the coast, such as the north of Russia near the Arctic Ocean, Russian Far East,

23   Korean peninsula, Northern Mediterranean and Northeast Canada. For NHSnow and GlobSnow, most

24   bias is distributed near the μ=0 line with high frequency, although some bias is greater than 100 (or less

25   than −100) (Fig. 5b, d). Positive (negative) biases indicate mean grid cell values less (greater) than

26   those of the respective stations SD measures. Fig. 5c showed the ERA-Interim/Land overestimate snow

27   depth in Western Siberian Plains and Eastern European Plains (around 60 °N; orange dots). As

1   reference, Average SD pattern of three products in February (1992-2010) were also provided in

2   Appendix (Fig. A)

3   For analysis indexes, MAE and RMSE, the distribution of error points of NHSnow and GlobSnow

4   are much the same as the distribution of its bias (Fig. 5-7).We used all evaluation records to calculate

5   three precision indexes for three products. We found that the bias, MAE and RMSE is 0.59 cm, 15.12

6   cm and 20.11 cm, respectively, for NHSnow gridded product, but more bias (1.19 cm), MAE (15.98 cm)

7   and lower RMSE (15.48 cm) for GlobSnow (Table 4). This comparison (NHSnow vs. GlobSnow)

8   showed relatively good agreement, although NHSnow over- or underestimated the SD with larger

9   RMSE. Overall, the performance of GlobSnow was better than the NHSnow gridded product. However,

10 part of the validation data were also applied for GlobSnow assimilation, it is highly possible that in this

11 case GlobSnow validation may not completely independent. The different performance for these two

12 products may be mainly because the evolution of snow grain size by HUT (The Helsinki University of

13 Technology) model was used to generate SWE in GlobSnow. Che et al. (2016) reported that the grain

14 size is more important than snow density and temperature. Further, ERA-Interim/Land had the worst

15 performance of all three products with highest bias (-5.60), MAE (18.72) and RMSE (37.77). The

16 smallest bias is located near mid-latitude regions (< 50 °N) and much of the bias lies at 0–100 cm for

17 ERA-Interim/Land products (Fig. 5e, f). It must be noted that there are 89 bias records in two stations,

18 which located in Novosibirsk Islands and Victoria Island, is much less than -300 cm (approximately

19 -3000 cm). Large MAE and RMSE can be found in high latitude and coastal region (Fig. 5e). Unlike

20 NHSnow and GlobSnow, ERA-Interim/Land is more likely to overestimate SD and appears to be less

21 consistent with in situ observation across the Northern Hemisphere (Fig. 5f). Through analyzing ground

22 observation, we can see that deep snow is distributed in high latitude areas.

23   While the gridded products do a fairly good job of representing smaller accumulations of SD

24 (shadow and mid-deep snow cover), they all struggle to capture very high accumulations (deep snow)

25 with less bias, MAE and RMSE (Fig. 5-7, Fig. A). As a result, variation in snow cover could fail to be

26 adequately captured in areas with frequent deep snow and, thus, we should be cautious when

27 interpreting of this validation result.

28   Uncertainties in these three gridded snow products caused by ground temperature and topographic

29 factor could result in some level discrepancies between the measured and the estimated SD (Vander

30 Jagt et al., 2013;Snauffer et al., 2016). Forests exhibit strong influence on snow distributions by canopy

1   interception and the evolution of snow properties. The dense portions of boreal forests are widely

2   distributed in NA and northern EU (Friedl et al., 2010) Large bias, MAE and RMSE regions of three

3   gridded products (Fig. 5-7) cover vast areas of tall vegetation (forests and shrub). Furthermore, the

4   spatial inhomogeneity cause one grid cells (~25 km) that is almost not possible to completely cover by

5   one vegetation type (low heterogeneity). Because the estimated SD of NHSnow depends on land cover

6   types, this discrepancy induced by surface cover heterogeneity could partly account for why NHSnow

7   has a smaller MAE and RMSE for low vegetation (bare-land and prairie) distributed at middle and low

8   latitudes, than the higher vegetation (shrub and forest) areas at higher latitudes (Xiao et al., 2018).

9   As well, there are scale mismatches between in situ observation and the gridded products with

10   regard to snowpack properties and their spatiotemporal representativeness (Frei et al., 2012). It is

11   difficult to precisely validate coarse-resolution satellite observation using ground truth. Subsequently,

12   over- or underestimates are inevitable when using a single in situ (SD or SWE) observation to test the

13   veracity of the gridded products (Mudryk et al., 2015;Xiao et al., 2018). Snow surveys would benefit

14   from multiple measurements at different points within one pixel (López-Moreno et al., 2011). In situ

15   observations are highly representative when the SD varies smoothly in space, and poorly representative

16   when the SD is spatially stepped (Che et al., 2016). However, there is almost always a lack of sufficient

17   ground-measured data. To date, field site observations are still to be more authentic and reliable

18   datasets than satellite observation.

19   As a whole, the accuracy of estimated SD in the Northern Hemisphere presented a spatial

20   heterogeneity. Issues of scale and spatial heterogeneity of validation data notwithstanding, these

21   comparisons conducted in our work can yield valuable insight into the performance of these products.

22   **4.1.2 Variation of snow depth**

23   To better understand and interpret snow cover variation across the Northern Hemisphere, we

24   conducted an analysis of SD variation using seasonal maximum SD from 1992–2016. According to the

25   rules of variation level grading, which was divided into 5 grade (extremely significant increase,

26   significant increase, non-significant change, extremely significant decrease, and significant decrease;

27   Table 5), we can easily gained seasonal maximum SD variation level range 1992 to 2016. Figure 8

28   shows the variation pattern of seasonal maximum SD in three seasons (fall, winter and spring) with

1   statistical significance level. In three seasons, variation trend of seasonal maximum SD exhibited a

2   distinctly different pattern over the Northern Hemisphere since 1992. Seasonal maximum SD variation

3   results in fall illustrated that a reduction trend account for most area of the EU with the rate ranging

4   from 0 to 1 cm yr.$^{-1}$. The Figure 8a show the significant level pattern of corresponding maximum SD

5   change trend. We can find that the area, which show extremely significant decrease in fall, are mainly

6   located in the Russian Far East, the Qinghai-Tibet Plateau, the southern Siberian Plateau, and the

7   northeastern region of Canada. On the contrary, Russia's Taimer Peninsula and the United States'

8   Alaska region shows extremely significant increase trend (0 ~1 cm yr.$^{-1}$). In addition, the maximum SD

9   in winter and spring also exhibited extremely significant decrease in the Qinghai-Tibet Plateau and the

10   northeastern region of Canada as shown in Figure 8b and 8c. The area with extremely significant

11   decrease trend extent add a Western Siberian plain region. Wang and Li (2012) used nearly 50a of daily

12   station SD observation data to analyze the trend of maximum SD in China. The variation trend of

13   seasonal maximum SD in the Qinghai-Tibet Plateau form previous study is consistent with the

14   conclusion observed in this study (Wang and Li, 2012).There are more regions in seasonal maximum

15   SD with extremely significant increase trend in winter and spring (green region). Furthermore, a

16   strange phenomenon that the variation trend of seasonal maximum SD in the Russian Far East show

17   extremely significant decrease, while it is in inverse in spring. This variation trend of maximum SD in

18   spring analyzed using NHSnow products is consistent with the analysis results using GlobSnow

19   products from recently published study (Wu et al., 2018). It need be pointed out that the significant

20   increase (decrease) area is located around extremely significant increase (decrease) as shown in Figure

21   8. No matter which season, although the variation trend of maximum seasonal SD didn't pass the

22   significance level test, we can draw the conclusion that the wide range of area across the Northern

23   Hemisphere experienced pronounced change during the period 1992 to 2016.

24   Finally, we analyzed season variation analysis of SD across the Northern Hemisphere using

25   seasonal average SD as analysis index. Seasonal average SD was defined as the cumulative SD divided

26   by the days in one snow cover season.SD variation rate fluctuated in different regions and seasons. It

27   was generally large in the region north of 55° N (Fig. 9, Fig. B and C in appendix). This fluctuation

28   was large in winter with high of −0.11 ± 0.40 cm yr.$^{-1}$ than other seasons during 1992–2016 (Fig. 9d,

29   Table 6.), which means that the maximum changes occurred in winter. Similar conclusion also can be

30   easily found in the two periods 1992–2001 and 2002–2016 (Fig. B-d, C-d and Table 6). Although not

1   all variation trends passed the significance test, most regions in the Northern Hemisphere show

2   increasing trends during 1992-2001 (Fig. B; Table 6). The SD variation trend in the three seasons

3   during 2002–2016 was reversed. The SD absolute variation rate during 2002–2016 is apparently greater

4   than its rate during 1992–2001 (Fig. C; Table 6). The last century were considered to be the warmest

5   period.

6   The high fluctuation of SD variation rate especially occurred in the polar region (the arctic and the

7   Tibetan plateau) for three seasons. In the context of global climate change, we found that winter SD

8   variation was more sensitive to climate change (Brown et al., 2010). The strength of this relationship is

9   spatially complex, varying by latitude, region, and climate condition.

10   **4.2 Total SWE**

11   GlobSnow dataset covers all land surface areas excluding mountainous regions, glaciers and

12   Greenland as described in Section 2.4. From above analysis, we can find that ERA-Interim/Land have

13   somewhat poor performance in SD estimation. Thus, further analysis of snow cover variation in the

14   Northern Hemisphere used NHSnow products as analysis data. The forecast for total SWE (or snow

15   mass) have great potential consequences on agriculture practices in many regions. Total SWE in here is

16   calculated by SWE multiplied by snow cover area (Qin et al., 2006). It should be noted that the snow

17   classification tree (Grody and Basist, 1996), which have been applied in many studies (Che et al.,

18   2008;Dai et al., 2017;Yu et al., 2012), was used to detect snow cover for NHSnow product. Liu et al.

19   (2018) also reported that Grody's algorithm had higher positive predictive values and lower omission

20   errors by testing snow cover mapping algorithms with the in situ SD over China. In this study, Annual

21   (or monthly average) total SWE, which is the sum of daily (or the mean of monthly) total SWE in one

22   snow cover year (or each month of 25 years).

23   Interannual variation (Fig. 10) and intra-annual cycles (not show figure) of total SWE over the

24   Northern Hemisphere were used to analyze total SWE variation characteristic over the past 25 years

25   (1992–2016). Figure 8 depicts the time series of interannual variation of total SWE anomaly with

26   respect to 1992–2016 reference period. The maximum anomaly occurred in 1998–1999 period with

27   the minimum was during 2015–2016. It present particularly significant decreasing trends ($P \leq 0.05$)

28   during 1992–2016, at the rate of approximately -5794 km^3 yr.$^{-1}$. Trend analysis reveals that total SWE

29   have 12.5% reduction from 1992 to 2016. There is a slow variation rate by about 710 km^3 yr.$^{-1}$ ($P >$

1   0.05) for 1992-2001 period. In contrast, the total SWE anomaly significant decrease (P ≤ 0.05) after

2   2002 at rate of approximately -9041 km³ yr.⁻¹, which may lead to a decreasing trends of total SWE

3   during 1992–2016. There was a sudden drop of total SWE in 2008–2009 as found in previous studies

4   (Derksen and Brown, 2012;Wang et al., 2018). However, other factors, for instance, oceanic and

5   atmospheric heat transport, sea ice season wind, and solar insolation anomalies, may have contributed

6   to the fluctuation of total SWE (Liu and Key, 2014). Variation of total SWE across the Northern

7   Hemisphere could well capture the variation characteristic of the Arctic sea ice extent (Tilling et al.,

8   2015).

9   When analyzing long-term variation of monthly average total SWE, ten months (September to

10   June) exhibit significant decreasing apart from March and April (Table 7). The maximum decrease

11   was approximately -1066 km³ yr.⁻¹ in January while the minimum decrease occurred in September at

12   -177 km³ yr.⁻¹. An increasing trend appears in March with a rate of approximately 68 km³ yr.⁻¹ (P >

13   0.05), however, relatively large decrement in fall and winter are unable to partially be offset by the

14   increment of March. Compared with the fall (September to November) and spring (February to June),

15   the interannual variability of monthly average total SWE significantly decreased in winter (December

16   to January), with average rate of less than -1000 km³ yr.⁻¹. We also found that the monthly average

17   total SWE reduction fluctuated ranging from -66% to -4% for each month (September to June) over

18   1992-2016 (Table 7). The largest and smallest reduction were about 65.8% and 4.2%, which occurred

19   in June and March, respectively.

20   Over large areas, it is extremely convenient to use remote sensing to infer SWE. Albeit there are

21   numerous ways to estimate SWE, it is very challenging to determine precise distributions of SWE at

22   regional and global scales (Chang et al., 1987;Kongoli, 2004;Tedesco and Narvekar, 2010;Bair et al.,

23   2018). Snow density, which can be used to convert SWE from SD, is potential and key factor in

24   accurate estimation of SWE (Sturm et al., 2010;Tedesco and Narvekar, 2010). In fact, snow density

25   typically varies from 0.05 g/cm³ for new snow at low air temperatures to over 0.55 g/cm³ for a ripened

26   snowpack (Anderton et al., 2004;Cordisco et al., 2006). Noteworthily, this study using dynamic snow

27   density to convert SD to SWE is based on the assumption that snowpack occurs as a single layer

28   (Sturm et al., 2010), to capture dynamic characteristics of snow property. The evolution of the

29   ephemeral snow class did not be provided by Sturm et al. (2010). The mean value (0.25 g/cm³) of snow

30   density of ephemeral snow (Zhong et al., 2014), which mean that without any evolution throughout the

The Cryosphere
Discussions

1   snow cover year. Meanwhile, this value for ephemeral snow was set as 0.2275 g/cm^3 in Tedesco and

2   Jeyaratnam (2016) study. Snow density also exhibits great heterogeneity in vertical direction, so that a

3   single layer of snow concept cannot fully capture the snowpack property. The density of the top

4   snowpack (fresh snow; ~ 0.10 g/cm^3) increases gradually from the top toward the bottom (Dai et al.,

5   2012). The bottom layer of snowpack is old undergoing compaction and grain size growth with a

6   relatively high density (0.3~0.6 g/cm^3). Although our snow density description strategy does not

7   completely describe the actual evolution in snow density, there is no better alternative.

8   **4.3 Snow cover days**

9   Snow cover days (SCD) is defined as the number of days in one snow cover year in which SD is

10   over 0 cm (Zhong, 2014). Snow cover year was defined as the period between July of a given year and

11   June of the following year (Xiao et al., 2018). A least-squares regression was used to analyze the

12   variation of SCD for each pixel from 24 snow cover years, with per-pixel evaluation of significance

13   (F-test).

14   We exploring the variation in SCD during 1992-2016. Most areas across the Northern Hemisphere

15   present a prominently decreasing trend at a rate ranging from 0 to 5 day yr.$^{-1}$ (Fig. 11a). Decreasing

16   regions are mainly distributed in EU. For example, north of Russia and large parts of central Asia. The

17   area that shows decreasing trends of SCD in EU is much larger than that in NA (Fig. 11a) (Derksen and

18   Brown, 2012). Areas that the decrease at a rate greater than 5 day yr.$^{-1}$ are almost all located in China,

19   such as North of Qilian Mountain, central Tibetan Plateau, and Tianshan Mountain. Areas that exhibits

20   increasing trends, can be found in central of NA, Western Europe, Northwestern Mongolia, and some

21   parts of China. Throughout the Northern Hemisphere (Fig. 11b), the decreasing trend covered most

22   parts of the regions (25 ~ 85 °N) with a mean decreasing rate of approximately 1.0 day yr.$^{-1}$. Latitudes

23   around 50 °N is an exception where variation is close to 0 day yr.$^{-1}$. The most notable variation trend

24   (decreasing or increasing) occurred over polar region (Fig. 11b). This may be because there are few

25   pixels in the polar mainland.

26   SCD variation rate also were divided into 5 grade (Table 5). Unlike SCD variation rate patterns,

27   the variation level pattern shows that the non-significant changes area dominates SCD variation trends

28   across the Northern Hemisphere (Fig. 11c). Extremely significant and significant decrease appear in

29   northwest of Hudson Bay in Canada, Kamchatka peninsula, Eastern European plains, the north of

1 Russia, Iranian plateau, and several regions in China (the Tibet Plateau, Tianshan Mountain and

2 Northeast China Plain). In addition, extremely significant and significant increase only occur in a

3 limited area of NA, eastern Tibet Plateau regions, and China's central and northern regions.

4   Interestingly, the opposite variation trends in SCD and SD appear in several regions. Maximum

5 SD in spring (Fig. 8c) and annual average SD (figure not shown) show extremely significant increasing

6 trends , whereas SCD exhibit extremely significant decreases in corresponding regions (Fig. 11c), such

7 as Central Siberian Plateau, Greater Khingan Mountains in China, and the eastern Scandinavian

8 Peninsula. This different variation trend of SD and SCD was also reported by Zhong et al. (2018) using

9 ground-based data. The primary reason may be the increase of frequency of extreme snowfall in which

10 SD could demonstrate on increasing trend. Additionally, a recent study found that the greater SWE, the

11 faster melting rate leading to a shortened SCD in Northern Hemisphere (Wu et al., 2018).

12   Despite the similarities between the station- and satellite-derived time series, it can be

13 demonstrated that Northern Hemisphere meteorological station data do not provide perfect large-scale

14 variation characteristics of ground snow cover (Zhong et al., 2018). Our analyses provide further

15 evidence supporting observations of significant decreasing trends in SCD occurring in the Northern

16 Hemisphere. Compared to SCD derived from optic sensors snow cover product, however, the specific

17 quantity of SCD and SCD variation rate derived from NHSnow SD data was overestimated (Wang et

18 al., 2018;Hori et al., 2017). The SCD variation trends derived from NHSnow product almost is same as

19 derived from optical snow cover product in variation pattern (Hori et al., 2017).

20   Since the optical (MODIS or AVHRR) and microwave sensors (SSM/I or AMSR-E) respond in

21 different parts of the electromagnetic spectrum, the estimated snow cover will to be somewhat vary.

22 The shallow snow could not induce volume scattering at 37 GHz, and thus passive microwave

23 observations often give better snow cover result at thick snow (>5 cm) (Foster et al., 2009;Wang et al.,

24 2008). The threshold for SCD definition in here is 0 cm, whereas it is 1 cm or larger in other studies

25 (Ke et al., 2016;Dyer and Mote, 2006). As well, another explanation for these discrepancy could be

26 snow cover identification algorithm (Liu et al., 2018;Hall et al., 2002).

27   The microwave radiation characteristics of snow cover is similar to that of precipitation, cold

28 desert and, frozen ground (Grody and Basist, 1996). Commission and omission errors in NHSnow

29 product may result from coarse spatial resolution, snow characteristics and topography according to

30 Dai et al. (2017), precipitation (Liu et al., 2018;Grody and Basist, 1996) especially over frozen ground

1   (Tsutsui and Koike, 2012). Algorithm several rules were used to distinguish snow from precipitation,

2   cold desert, and frozen ground (Xiao et al., 2018), it is impossible to entirely remove interference

3   factors in each image. Additionally, the precondition of NHSnow is dry snow, which mean almost no

4   wet snow was considered into SCD variation analysis (Singh and Gan, 2000). The poorer performance

5   of the microwave derived products was anticipated because of documented difficulties monitoring

6   snow cover over forested and mountainous terrain (Vander Jagt et al., 2013;Smith and Bookhagen,

7   2016).

8   **5 Conclusions**

9   This project applied the SVR SD retrieval algorithm proposed by Xiao et al (2018), which using

10 PM remote sensing and other auxiliary data, to develop a long term (from January 1992 to December

11 2016) Northern Hemisphere daily SD and SWE products (NHSnow) with 25-km spatial resolution. We

12 then analyzed the spatial and temporal change in snow cover (SD, total SWE and, SCD) across the

13 Northern Hemisphere, and quantified the magnitude of variation of snow cover using SD and SWE

14 extracted from NHSnow product.

15   In this study, we validated and compared among daily gridded products (NHSnow, GlobSnow and

16 ERA-Interim/Land) against ground snow-depth observations. The results show relatively high

17 estimation accuracy of SD from NHSnow, providing the relatively little bias, RMSE, and MAE

18 between the newly SD products and in situ observation. Analysis of SD variation revealed that the

19 variation rate ranging from 0 to 1 cm yr.$^{-1}$ (negative and positive) dominates the change in the Northern

20 Hemisphere, and the maximum changes appear in winter. Additionally, the results revealed the overall

21 SD trends in three seasons show increasing trend during 1992–2001, however it has a decreasing trend

22 during 2002–2016. Similar conclusions also appear in total SWE change analysis. The total SWE

23 shows a 12.5% reduction and the monthly average total SWE is 65.8% for the largest reduction and a

24 4.2% for least reduction which occur in June and March, respectively. The total SWE report

25 well-documented significant decreasing trends ($P < 0.05$) during the study period. Regression analysis

26 multi-year Northern Hemisphere SCD exhibits a prominent decreasing trend at a rate ranging from 0 to

27 5 day yr.$^{-1}$. The area of decreasing trends of SCD in EU is much larger than in NA. Unlike the SCD

28 variation rate, its variation level shows that non-significant changes areas dominate the variation

1 pattern across the Northern Hemisphere. An abnormal and interesting phenomenon is that opposite

2 SCD and SD variation trends appear in several regions.

3 While this study shed light on the spatiotemporal variability trends of snow cover across the

4 Northern Hemisphere using 25-year NHSnow product, we cannot claim NHSnow dataset could

5 completely capture the climate change signal in each region and season. Because of the deficiencies

6 and limitations (e.g. overestimation, underestimation), further efforts should be made to improve the

7 estimation accuracy and robustness of the SD inversion algorithm. Additionally, when more reliable

8 and numerous data become available, we will do more comprehensive validation over higher latitudes

9 and mountainous regions (Dai et al., 2017). Meanwhile, the validation analysis also should be carried

10 out in complex terrain and different land cover types (Tennant et al., 2017;Snauffer et al., 2016). It is

11 recommended that future work focus on the climatic effects and climatological causes in snow cover

12 changes to comprehensively understand the associated snow cover change mechanisms against a

13 climate change background (Huang et al., 2017;Flanner et al., 2011;Cohen et al., 2012).

14 **Acknowledgments**

1   **Appendix**
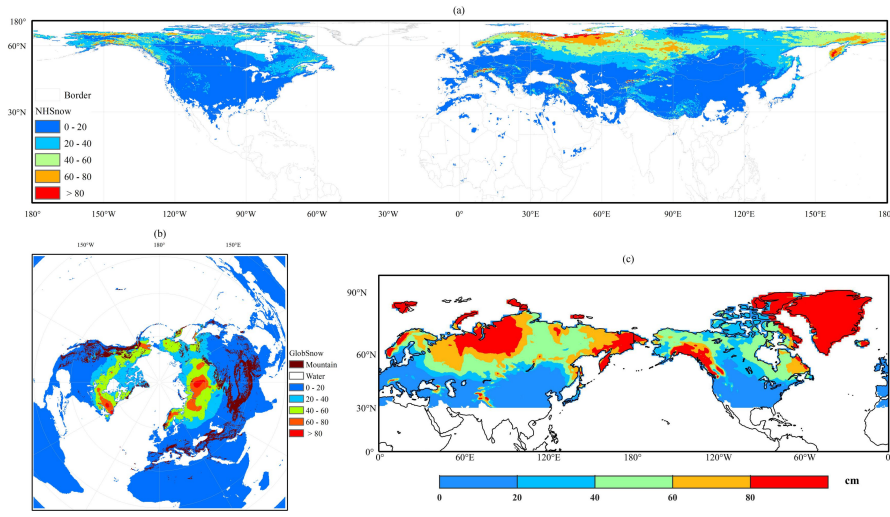
3   Figure A. Monthly average snow depth climatology of three products in February during 1992-2010: a)

4   NHSnow; b) GlobSnow, c) ERA-Interim/Land

5
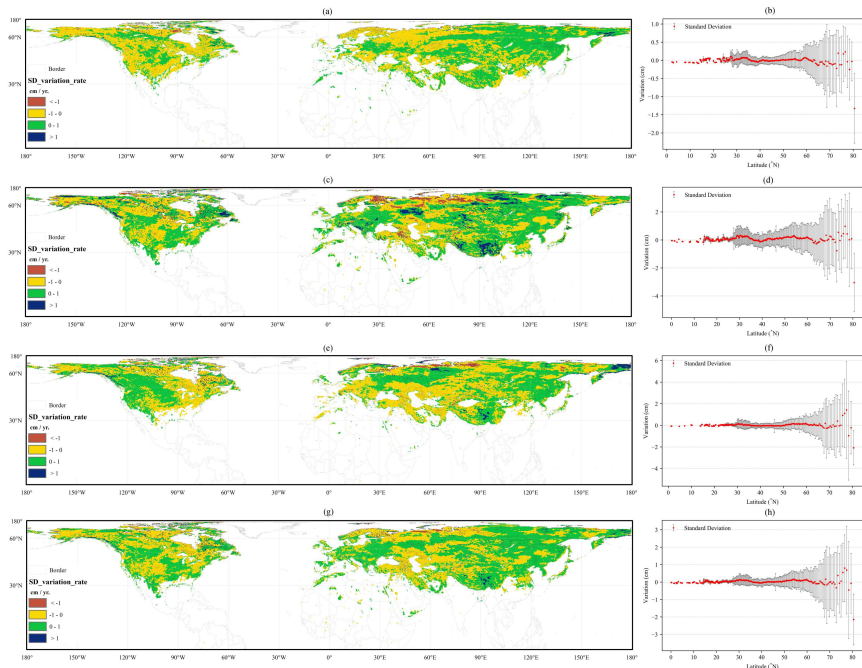
6

1   Figure B. The variation rate pattern of annual average (season) SD over the Northern Hemisphere for

2   three snow cover season, fall (a, b; September to November), winter (c, d; December to February),

3   spring (e, f; March to June) from 1992-2001. Black dots in (a, c, e, g) indicate that the changes are

4   significant at 95% confidence level (CL). The zonal distribution in (b, d, f, h) are mapped at 0.25

5   degree resolution in latitude. The error bars in (b, d, f, h) is one times of standard deviation.
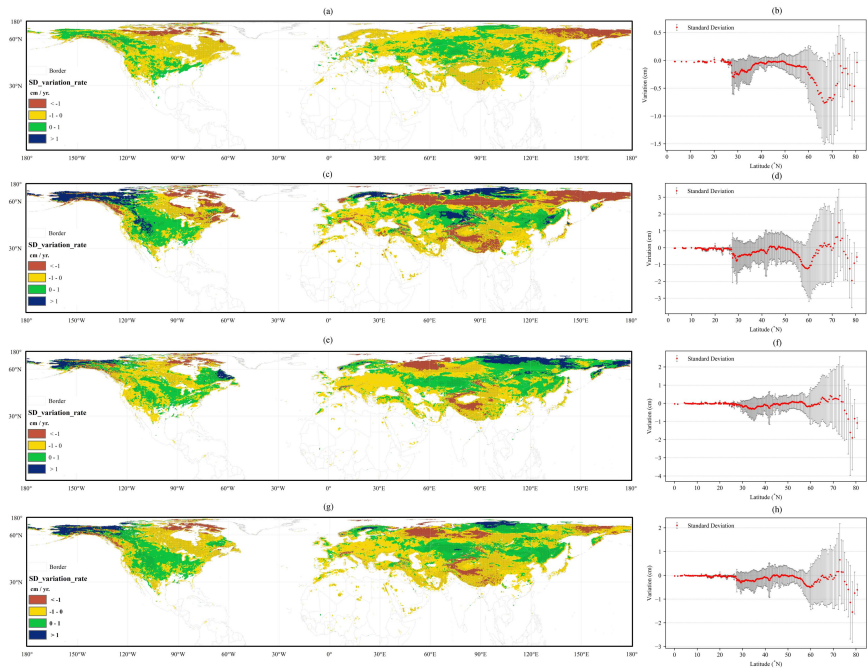
6

7   Figure C. The variation rate pattern of annual (season) average SD over the Northern Hemisphere for

8   three snow cover season, fall (a, b; September to November), winter (c, d; December to February),

9   spring (e, f; March to June) from 2002-2016. Black dots in (a, c, e, g) indicate that the changes are

10   significant at 95% confidence level (CL). The zonal distribution in (b, d, f, h) are mapped at 0.25

11   degree resolution in latitude. The error bars in (b, d, f, h) is one times of standard deviation.

12

1   Table A. AVHRR Global Land Cover classification and reclassification schemes

Value	Classification Label	Reclassification Label
0	Water	Water
1	Evergreen needle leaf forest	Forest
2	Evergreen broad leaf forest	
3	Deciduous needle leaf forest	
4	Deciduous broad leaf forest	
5	Mixed forest	
6	Woodland	
7	Wooded grassland	Prairie (Grassland)
10	Grassland	
8	Closed shrub land	Shrub
9	Open shrub land	
11	Cropland	Bare-land
12	Bare ground	
13	Urban and built	

2

References

Amante, C., Eakins, B.W.: ETOPO1 1 arc-minute global relief model: procedures, data sources and analysis, US Department of Commerce, National Oceanic and Atmospheric Administration, National Environmental Satellite, Data, and Information Service, National Geophysical Data Center, Marine Geology and Geophysics Division Colorado, 2009.

Anderton, S. P., White, S. M., and Alvera, B.: Evaluation of spatial variability in snow water equivalent for a high mountain catchment, Hydrological Processes, 18, 435-453, 10.1002/hyp.1319, 2004.

Armstrong, R., and Brodzik, M.: An earth-gridded SSM/I data set for cryospheric studies and global change monitoring, Advances in Space Research, 16, 155-163, 1995.

Armstrong, R. L., Knowles, K.W., Brodzik, M.J., Hardman, M.A.: DMSP SSM/I pathfinder daily EASE-grid brightness temperatures, Boulder, Colorado USA: National snow and ice data center, Digital media, 2008.

Bair, E. H., Andre Calfa, A., Rittger, K., and Dozier, J.: Using machine learning for real-time estimates of snow water equivalent in the watersheds of Afghanistan, The Cryosphere, 12, 1579-1594, 10.5194/tc-12-1579-2018, 2018.

Balsamo, G., Albergel, C., Beljaars, A., Boussetta, S., Brun, E., Cloke, H., Dee, D., Dutra, E., Munoz-Sabater, J., and Papenberger, F.: ERA-Interim/Land: A global land surface reanalysis dataset, European Geosciences Union General Assembly, 2015, 389-407,

Barnett, T. P., Adam, J. C., and Lettenmaier, D. P.: Potential impacts of a warming climate on water availability in snow-dominated regions, Nature, 438, 303-309, 10.1038/nature04141, 2005.

Barrett, B. S., Henderson, G. R., and Werling, J. S.: The Influence of the MJO on the Intraseasonal Variability of Northern Hemisphere Spring Snow Depth, Journal of Climate, 28, 7250-7262, 10.1175/jcli-d-15-0092.1, 2015.

Bilello, M. A.: Regional and seasonal variations in snow-cover density in the U.S.S.R, 1984.

Brodzik, M. J., and Knowles, K.: EASE-Grid: A Versatile Set of Equal-Area Projections and Grids, 2002.

Brown, R., Derksen, C., and Wang, L.: A multi-data set analysis of variability and change in Arctic spring snow cover extent, 1967–2008, Journal of Geophysical Research, 115, 10.1029/2010jd013975, 2010.

Brown, R., and Robinson, D.: Northern Hemisphere spring snow cover variability and change over 1922–2010 including an assessment of uncertainty, The Cryosphere, 5, 219-229, 2011.

Brown, R. D., and Frei, A.: Comment on "Evaluation of surface albedo and snow cover in AR4 coupled models" by A. Roesch, Journal of Geophysical Research, 112, 10.1029/2006jd008339, 2007.

Chang, A., Foster, J., and Hall, D.: Nimbus-7 SMMR derived global snow cover parameters, Ann. Glaciol, 9, 39-44, 1987.

Che, T., Xin, L., Jin, R., Armstrong, R., and Zhang, T.: Snow depth derived from passive microwave remote-sensing data in China, Annals of Glaciology, 49, 145-154, 2008.

Che, T., Dai, L., Zheng, X., Li, X., and Zhao, K.: Estimation of snow depth from passive microwave brightness temperature data in forest regions of northeast China, Remote Sensing of Environment, 183, 334-349, 2016.

Cohen, J. L., Furtado, J. C., Barlow, M. A., Alexeev, V. A., and Cherry, J. E.: Arctic warming, increasing snow cover and widespread boreal winter cooling, Environmental Research Letters, 7, 10.1088/1748-9326/7/1/014007, 2012.

Cordisco, E., Prigent, C., and Aires, F.: Snow characterization at a global scale with passive microwave

The Cryosphere
Discussions

1   satellite observations, Journal of Geophysical Research, 111, 10.1029/2005jd006773, 2006.

2   Dai, L., Che, T., Wang, J., and Zhang, P.: Snow depth and snow water equivalent estimation from
3   AMSR-E data based on a priori snow characteristics in Xinjiang, China, Remote Sensing of
4   Environment, 127, 14-29, 2012.

5   Dai, L., Che, T., and Ding, Y.: Inter-calibrating SMMR, SSM/I and SSMI/S data to improve the
6   consistency of snow-depth products in China, Remote Sensing, 7, 7212-7230, 2015.

7   Dai, L., Che, T., Ding, Y., and Hao, X.: Evaluation of snow cover and snow depth on the
8   Qinghai–Tibetan Plateau derived from passive microwave remote sensing, The Cryosphere, 11,
9   1933-1948, 10.5194/tc-11-1933-2017, 2017.

10   Derksen, C., Walker, A., and Goodison, B.: Evaluation of passive microwave snow water equivalent
11   retrievals across the boreal forest/tundra transition of western Canada, Remote Sensing of Environment,
12   96, 315-327, 2005.

13   Derksen, C., and Brown, R.: Spring snow cover extent reductions in the 2008-2012 period exceeding
14   climate model projections, Geophysical Research Letters, 39, n/a-n/a, 10.1029/2012gl053387, 2012.

15   Diffenbaugh, N. S., Scherer, M., and Ashfaq, M.: Response of snow-dependent hydrologic extremes to
16   continued global warming, Nat Clim Chang, 3, 379-384, 10.1038/nclimate1732, 2013.

17   Dutra, E., Balsamo, G., Viterbo, P., Miranda, P. M. A., Beljaars, A., Schär, C., and Elder, K.: An
18   improved snow scheme for the ECMWF land surface model: description and offline validation, Journal
19   of Hydrometeorology, 11, 899-916, 2010.

20   Dyer, J. L., and Mote, T. L.: Spatial variability and trends in observed snow depth over North America,
21   Geophysical Research Letters, 33, 10.1029/2006gl027258, 2006.

22   Flanner, M. G., Shell, K. M., Barlage, M., Perovich, D. K., and Tschudi, M. A.: Radiative forcing and
23   albedo feedback from the Northern Hemisphere cryosphere between 1979 and 2008, Nature
24   Geoscience, 4, 151-155, 10.1038/ngeo1062, 2011.

25   Forman, B. A., Reichle, R. H., and Derksen, C.: Estimating Passive Microwave Brightness Temperature
26   Over Snow-Covered Land in North America Using a Land Surface Model and an Artificial Neural
27   Network, IEEE Transactions on Geoscience & Remote Sensing, 52, 235-248, 2013.

28   Forman, B. A., and Reichle, R. H.: Using a support vector machine and a land surface model to
29   estimate large-scale passive microwave brightness temperatures over snow-covered land in North
30   America, IEEE Journal of Selected Topics in Applied Earth Observations and Remote Sensing, 8,
31   4431-4441, 2015.

32   Foster, J., Chang, A., and Hall, D.: Comparison of snow mass estimates from a prototype passive
33   microwave snow algorithm, a revised algorithm and a snow depth climatology, Remote sensing of
34   environment, 62, 132-142, 1997.

35   Foster, J. L., Hall, D. K., Kelly, R. E. J., and Chiu, L.: Seasonal snow extent and snow mass in South
36   America using SMMR and SSM/I passive microwave data (1979–2006), Remote Sensing of
37   Environment, 113, 291-305, 10.1016/j.rse.2008.09.010, 2009.

38   Foster, J. L., Hall, D. K., Eylander, J. B., Riggs, G. A., Nghiem, S. V., Tedesco, M., Kim, E., Montesano,
39   P. M., Kelly, R. E. J., Casey, K. A., and Choudhury, B.: A blended global snow product using visible,
40   passive microwave and scatterometer satellite data, International Journal of Remote Sensing, 32,
41   1371-1395, 10.1080/01431160903548013, 2011.

42   Frei, A., Tedesco, M., Lee, S., Foster, J., Hall, D. K., Kelly, R., and Robinson, D. A.: A review of global
43   satellite-derived   snow   products,   Advances   in   Space   Research,   50,   1007-1029,
44   10.1016/j.asr.2011.12.021, 2012.

1 Friedl, M. A., Sulla-Menashe, D., Tan, B., Schneider, A., Ramankutty, N., Sibley, A., and Huang, X.:
2 MODIS Collection 5 global land cover: Algorithm refinements and characterization of new datasets,
3 Remote Sensing of Environment, 114, 168-182, 2010.
4 Friedl, M. A., and Sulla-Menashe, D.: Note to users of MODIS Land Cover (MCD12Q1) Products,
5 Report. Accessed March, 2, 2014, 2011.
6 Gan, T. Y., Barry, R. G., Gizaw, M., Gobena, A., and Balaji, R.: Changes in North American snowpacks
7 for 1979–2007 detected from the snow water equivalent data of SMMR and SSM/I passive microwave
8 and related climatic factors, Journal of Geophysical Research: Atmospheres, 118, 7682-7697, 2013.
9 Gharaei-Manesh, S., Fathzadeh, A., and Taghizadeh-Mehrjardi, R.: Comparison of artificial neural
10 network and decision tree models in estimating spatial distribution of snow depth in a semi-arid region
11 of Iran, Cold Regions Science and Technology, 122, 26-35, 2016.
12 Goïta, K., Walker, A. E., and Goodison, B. E.: Algorithm development for the estimation of snow water
13 equivalent in the boreal forest using passive microwave data, International Journal of Remote Sensing,
14 24, 1097-1102, 2003.
15 Grippa, M., Mognard, N., Le Toan, T., and Josberger, E.: Siberia snow depth climatology derived from
16 SSM/I data using a combined dynamic and static algorithm, Remote sensing of environment, 93, 30-41,
17 2004.
18 Grody, N. C., and Basist, A. N.: Global identification of snowcover using SSM/I measurements, IEEE
19 Transactions on geoscience and remote sensing, 34, 237-249, 1996.
20 Hall, D. K., Kelly, R. E. J., Riggs, G. A., Chang, A. T. C., and Foster, J. L.: Assessment of the relative
21 accuracy of hemispheric-scale snow-cover maps, Annals of Glaciology, 34, 24-30, 2002.
22 Hancock, S., Baxter, R., Evans, J., and Huntley, B.: Evaluating global snow water equivalent products
23 for   testing   land   surface   models,   Remote   sensing   of   environment,   128,   107-117,
24 10.1016/j.rse.2012.10.004, 2013.
25 Hansen, M. C., Defries, R. S., Townshend, J. R. G., and Sohlberg, R.: Global land cover classification
26 at 1 km spatial resolution using a classification tree approach, International Journal of Remote Sensing,
27 21, 1331-1364, 2000.
28 Hori, M., Sugiura, K., Kobayashi, K., Aoki, T., Tanikawa, T., Kuchiki, K., Niwano, M., and Enomoto,
29 H.: A 38-year (1978–2015) Northern Hemisphere daily snow cover extent product derived using
30 consistent objective criteria from satellite-borne optical sensors, Remote Sensing of Environment, 191,
31 402-418, 10.1016/j.rse.2017.01.023, 2017.
32 Huang, X., Deng, J., Ma, X., Wang, Y., Feng, Q., Hao, X., and Liang, T.: Spatiotemporal dynamics of
33 snow cover based on multi-source remote sensing data in China, The Cryosphere, 10, 2453-2463,
34 10.5194/tc-10-2453-2016, 2016.
35 Huang, X., Deng, J., Wang, W., Feng, Q., and Liang, T.: Impact of climate and elevation on snow cover
36 using integrated remote sensing snow products in Tibetan Plateau, Remote Sensing of Environment,
37 190, 274-288, 10.1016/j.rse.2016.12.028, 2017.
38 Immerzeel, W. W., Van Beek, L. P., and Bierkens, M. F.: Climate Change Will Affect the Asian Water
39 Towers, Science, 328, 1382-1385, 2010.
40 Ke, C.-Q., Li, X.-C., Xie, H., Ma, D.-H., Liu, X., and Kou, C.: Variability in snow cover phenology in
41 China   from   1952   to   2010,   Hydrology   and   Earth   System   Sciences,   20,   755-770,
42 10.5194/hess-20-755-2016, 2016.
43 Kongoli, C.: Interpretation of AMSU microwave measurements for the retrievals of snow water
44 equivalent and snow depth, Journal of Geophysical Research, 109, 10.1029/2004jd004836, 2004.

1 Li, W., Guo, W., Qiu, B., Xue, Y., Hsu, P. C., and Wei, J.: Influence of Tibetan Plateau snow cover on
2 East Asian atmospheric circulation at medium-range time scales, Nat Commun, 9, 4243,
3 10.1038/s41467-018-06762-5, 2018.

4 Liang, J., Liu, X., Huang, K., Li, X., Shi, X., Chen, Y., and Li, J.: Improved snow depth retrieval by
5 integrating microwave brightness temperature and visible/infrared reflectance, Remote Sensing of
6 Environment, 156, 500-509, 2015.

7 Liu, X., Jiang, L., Wu, S., Hao, S., Wang, G., and Yang, J.: Assessment of Methods for Passive
8 Microwave Snow Cover Mapping Using FY-3C/MWRI Data in China, Remote Sensing, 10,
9 10.3390/rs10040524, 2018.

10 Liu, Y., and Key, J. R.: Less winter cloud aids summer 2013 Arctic sea ice return from 2012 minimum,
11 Environmental Research Letters, 9, 10.1088/1748-9326/9/4/044002, 2014.

12 López-Moreno, J. I., Fassnacht, S. R., Beguería, S., and Latron, J. B. P.: Variability of snow depth at the
13 plot scale: implications for mean depth estimation and sampling strategies, The Cryosphere, 5, 617-629,
14 10.5194/tc-5-617-2011, 2011.

15 Mudryk, L. R., Derksen, C., Kushner, P. J., and Brown, R.: Characterization of Northern Hemisphere
16 Snow Water Equivalent Datasets, 1981–2010, Journal of Climate, 28, 8037-8051,
17 10.1175/jcli-d-15-0229.1, 2015.

18 Pulliainen, J.: Mapping of snow water equivalent and snow depth in boreal and sub-arctic zones by
19 assimilating space-borne microwave radiometer data and ground-based observations, Remote Sensing
20 of Environment, 101, 257-269, 2006.

21 Qin, D., Liu, S., and Li, P.: Snow cover distribution, variability, and response to climate change in
22 western China, J. Climate, 19, 1820-1833, 2006.

23 Robinson, D. A., and Frei, A.: Seasonal variability of Northern Hemisphere snow extent using visible
24 satellite data, The Professional Geographer, 52, 307-315, 2000.

25 Rupp, D. E., Mote, P. W., Bindoff, N. L., Stott, P. A., and Robinson, D. A.: Detection and Attribution of
26 Observed Changes in Northern Hemisphere Spring Snow Cover, Journal of Climate, 26, 6904-6914,
27 10.1175/jcli-d-12-00563.1, 2013.

28 Singh, P. R., and Gan, T. Y.: Retrieval of snow water equivalent using passive microwave brightness
29 temperature data, Remote Sensing of Environment, 74, 275-286, 2000.

30 Smith, T., and Bookhagen, B.: Assessing uncertainty and sensor biases in passive microwave data
31 across High Mountain Asia, Remote Sensing of Environment, 181, 174-185, 2016.

32 Snauffer, A. M., Hsieh, W. W., and Cannon, A. J.: Comparison of gridded snow water equivalent
33 products with in situ measurements in British Columbia, Canada, Journal of Hydrology, 541, 714-726,
34 10.1016/j.jhydrol.2016.07.027, 2016.

35 Sturm, M., Holmgren, J., and Liston, G. E.: A seasonal snow cover classification system for local to
36 global applications, Journal of Climate, 8, 1261-1283, 1995.

37 Sturm, M., Taras, B., Liston, G. E., Derksen, C., Jonas, T., and Lea, J.: Estimating snow water
38 equivalent using snow depth data and climate classes, Journal of Hydrometeorology, 11, 1380-1394,
39 2010.

40 Sturm, M.: White water: Fifty years of snow research in WRR and the outlook for the future, Water
41 Resources Research, 51, 4948-4965, 10.1002/2015wr017242, 2015.

42 Takala, M., Luojus, K., Pulliainen, J., Derksen, C., Lemmetyinen, J., Kärnä, J.-P., Koskinen, J., and
43 Bojkov, B.: Estimating northern hemisphere snow water equivalent for climate research through
44 assimilation of space-borne radiometer data and ground-based measurements, Remote Sensing of

The Cryosphere
Discussions

Open Access

EGU

1 Environment, 115, 3517-3529, 2011.

2 Tedesco, M., Pulliainen, J., Takala, M., Hallikainen, M., and Pampaloni, P.: Artificial neural

3 network-based techniques for the retrieval of SWE and snow depth from SSM/I data, Remote sensing

4 of Environment, 90, 76-85, 2004.

5 Tedesco, M., and Narvekar, P. S.: Assessment of the NASA AMSR-E SWE Product, IEEE Journal of

6 Selected Topics in Applied Earth Observations and Remote Sensing, 3, 141-159, 2010.

7 Tedesco, M., Derksen, C., Deems, J. S., and Foster, J. L.: Remote sensing of snow depth and snow

8 water equivalent, Remote Sensing of the Cryosphere, 73-98, 2014.

9 Tedesco, M., and Jeyaratnam, J.: A New Operational Snow Retrieval Algorithm Applied to Historical

10 AMSR-E Brightness Temperatures, Remote Sensing, 8, 2016.

11 Tennant, C. J., Harpold, A. A., Lohse, K. A., Godsey, S. E., Crosby, B. T., Larsen, L. G., Brooks, P. D.,

12 Kirk, R. W. V., and Glenn, N. F.: Regional sensitivities of seasonal snowpack to elevation, aspect, and

13 vegetation cover in western North America, Water Resources Research, 53, 2017.

14 Tilling, R. L., Ridout, A., Shepherd, A., and Wingham, D. J.: Increased Arctic sea ice volume after

15 anomalously low melting in 2013, Nature Geoscience, 8, 643-646, 10.1038/ngeo2489, 2015.

16 Tsutsui, H., and Koike, T.: Development of Snow Retrieval Algorithm Using AMSR-E for the BJ

17 Ground-Based Station on Seasonally Frozen Ground at Low Altitude on the Tibetan Plateau, Journal of

18 the Meteorological Society of Japan. Ser. II, 90C, 99-112, 10.2151/jmsj.2012-C07, 2012.

19 Vander Jagt, B. J., Durand, M. T., Margulis, S. A., Kim, E. J., and Molotch, N. P.: The effect of spatial

20 variability on the sensitivity of passive microwave measurements to snow water equivalent, Remote

21 Sensing of Environment, 136, 163-179, 2013.

22 Wang, C., and Li, D.: Spatial-temporal variations of snow cover days and the maximum depth of snow

23 cover in China during recent 50 years, Journal of Glaciology and Geocryology, 34, 247-256, 2012.

24 Wang, X., Xie, H., and Liang, T.: Evaluation of MODIS snow cover and cloud mask and its application

25 in Northern Xinjiang, China, Remote Sensing of Environment, 112, 1497-1513,

26 10.1016/j.rse.2007.05.016, 2008.

27 Wang, Y., Huang, X., Liang, H., Sun, Y., Feng, Q., and Liang, T.: Tracking Snow Variations in the

28 Northern Hemisphere Using Multi-Source Remote Sensing Data (2000–2015), Remote Sensing, 10,

29 10.3390/rs10010136, 2018.

30 Wegmann, M., Orsolini, Y., Dutra, E., Bulygina, O., Sterin, A., and Brönnimann, S.: Eurasian snow

31 depth in long-term climate reanalyses, The Cryosphere, 11, 923-935, 10.5194/tc-11-923-2017, 2017.

32 Wentz, F. J.: SSM/I version-7 calibration report, Remote Sensing Systems Tech. Rep, 11012, 46, 2013.

33 Wu, X., Che, T., Li, X., Wang, N., and Yang, X.: Slower Snowmelt in Spring Along With Climate

34 Warming Across the Northern Hemisphere, Geophysical Research Letters, 45, 12,331-312,339,

35 10.1029/2018gl079511, 2018.

36 Xiao, X., Zhang, T., Zhong, X., Shao, W., and Li, X.: Support vector regression snow-depth retrieval

37 algorithm using passive microwave remote sensing data, Remote Sensing of Environment, 210, 48–64,

38 2018.

39 Xu, X., Liu, X., Li, X., Xin, Q., Chen, Y., Shi, Q., and Ai, B.: Global snow cover estimation with

40 Microwave Brightness Temperature measurements and one-class in situ observations, Remote Sensing

41 of Environment, 182, 227-251, 2016.

42 Xue, Y., and Forman, B. A.: Comparison of passive microwave brightness temperature prediction

43 sensitivities over snow-covered land in North America using machine learning algorithms and the

44 Advanced Microwave Scanning Radiometer, Remote Sensing of Environment, 170, 153-165, 2015.

1   Ye, H., Cho, H.-r., and Gustafson, P. E.: changes in russian winter snow accumulation during 1936-83
2   and its spatial patterns, Journal of Climate, 11, 856-863, 1998.
3   Yu, H., Zhang, X., Liang, T., Xie, H., Wang, X., Feng, Q., and Chen, Q.: A new approach of dynamic
4   monitoring of 5‐day snow cover extent and snow depth based on MODIS and AMSR‐E data from
5   Northern Xinjiang region, Hydrological Processes, 26, 3052-3061, 2012.
6   Zhang, T., Osterkamp, T., and Stamnes, K.: Influence of the depth hoar layer of the seasonal snow
7   cover on the ground thermal regime, Water Resources Research, 32, 2075-2086, 1996.
8   Zhang, T.: Influence of the seasonal snow cover on the ground thermal regime: An overview, Reviews
9   of Geophysics, 43, 589-590, 2005.
10   Zhang, Y., Li, T., and Wang, B.: Decadal Change of the Spring Snow Depth over the Tibetan Plateau_
11   The Associated Circulation and Influence on the East Asian Summer Monsoon, Journal of Climate, 17,
12   2780-2793, 2004.
13   Zhong, X.: Spatiotemporal variability of snow cover and the relationship between snow and climate
14   change across the Eurasian Contient, Lanzhou: Cold and Arid Regions Environmental and Engineering
15   Research Institute, CAS, 2014.
16   Zhong, X., Zhang, T., and Wang, K.: Snow density climatology across the former USSR, The
17   Cryosphere, 8, 785-799, 2014.
18   Zhong, X., Zhang, T., Kang, S., Wang, K., Zheng, L., Hu, Y., and Wang, H.: Spatiotemporal variability
19   of snow depth across the Eurasian continent from 1966 to 2012, The Cryosphere, 12, 227-245,
20   10.5194/tc-12-227-2018, 2018.
21

The Cryosphere
Discussions

Open Access

EGU

1 **List of Tables and Figures**

2 Table 1 Detail description for SSM/ and SSMIS sensors. H and V denotes horizontal and vertical

3 polarization, respectively.

Satellite	SSM/I		SSMIS
Platform	F 11	F 13	F 17
Temporal coverage	1991.12-1995.5	1995.5-2008.6	2006.12 -
Channels (GHz)	19 H, V; 22 V; 37 H, V; 85 H, V		19 H, V; 22 V; 37 H, V; 91 H, V

4

5 Table 2. Training sample filter rules

Layer ID	Filter rules
Layer2.	If $\text{Number}_{total}(layer2) \leq 3000$ $\text{Number}_{training}(layer2) = (\text{Number}_{total}(layer2))/2$ Else $\text{Number}_{training}(layer2) = 3000$
Layer3.	If $\text{Number}_{total}(layer3) \leq 3000$ $\text{Number}_{training}(layer3) = (\text{Number}_{total}(layer3))/2$ Else $\text{Number}_{training}(layer3) = 3000$
Layer1.	If $\text{Number}_{training}(layer2) > 2000$ or $\text{Number}_{training}(layer3) > 1000$ $\text{Number}_{training}(layer1)$ $\qquad = 15000 - \text{Number}_{training}(layer2) - \text{Number}_{training}(layer3)$ Else $\text{Number}_{training}(layer1) = 12000$

6

7 Table 3 Snow density estimation model parameters

Snow class	ρ_{max}	ρ_0	k_1	k_2	References
Alpine	0.5975	0.2237	0.0012	0.0038	
Maritime	0.5979	0.2578	0.0010	0.0038	
Prairie	0.5940	0.2332	0.0016	0.0031	Sturm et al. (2010)
Tundra	0.3630	0.2425	0.0029	0.0049	
Taiga	0.2170	0.2170	0	0	
Ephemeral	0.2500	0.2500	0	0	Zhong et al. (2014)

8

Table 4. The evaluated indexes (bias, MAE, RMSE; unit: cm) for three gridded SD products (NHSnow, GlobSnow, ERA-Interim/Land).

Products	Bias	MAE	RMSE
NHSnow	0.59	15.12	20.11
GlobSnow	1.19	15.98	15.48
ERA-Interim/Land	-5.60	18.72	37.77

Table 5. Rules of variation level grading

Variation rate	P value	Variation level
rate > 0	$p \leq 0.01$	extremely significant increase
rate > 0	$0.01 < p \leq 0.05$	significant increase
-	$P > 0.05$	non-significant change
rate < 0	$p \leq 0.01$	extremely significant decrease
rate < 0	$0.01 < p \leq 0.05$	significant decrease

Table 6. Mean variation rate of average SD (cm yr.$^{-1}$) over the Northern Hemisphere for three common period (1992-2016, 1992-2001, 2002-1996) and snow cover seasons (fall, winter, spring). Std. means standard deviation

Season	1992-2016 (Mean ± 1 Std.)	1992-2001 (Mean ± 1 Std.)	2002-2016 (Mean ± 1 Std.)
Fall	-0.08 ± 0.11	-0.01 ± 0.19	-0.15 ± 0.22
Winter	-0.11 ± 0.40	0.06 ± 0.62	-0.22 ± 0.75
Spring	-0.04 ± 0.25	0.02 ± 0.51	-0.07 ± 0.41
Year	-0.06 ± 0.20	0.02 ± 0.35	-0.11 ± 0.34

Table 7. Variation rate and changes of monthly average total SWE. The asterisk indicate that the changes are significant at 95% confidence level

Month	Variation rate (km^3/yr.)	% Change in the mean of monthly average total SWE over 1992-2016 period
September	-176.66*	-63.73%

October	-776.92*	-43.95%
November	-1060.10*	-26.83%
December	-979.71*	-4.82%
January	-1065.72*	-9.53%
February	-838.79*	-9.52%
March	67.54	-4.17%
April	-128.04	-6.44%
May	-343.55*	-20.34%
June	-226.01*	-65.79%

1

2
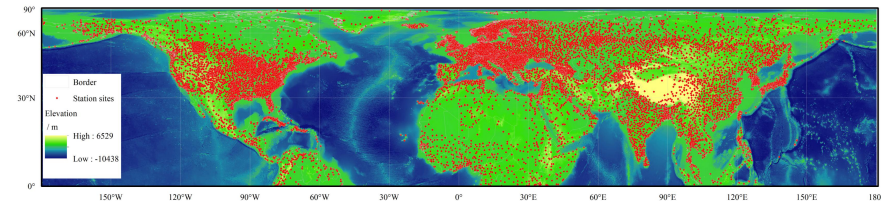
Figure 1. Distribution of Meteorological stations overlaid on ETOPO1 in the Northern Hemisphere.

5
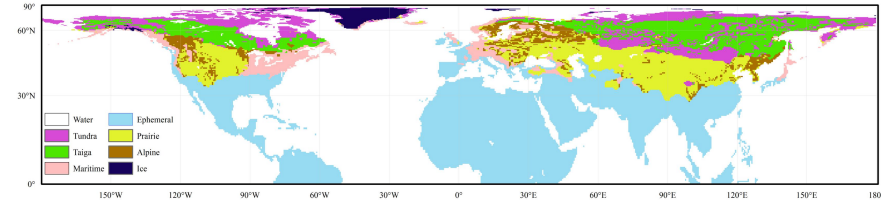
Figure 2. Snow Class distribution in the Northern Hemisphere

The Cryosphere
Discussions
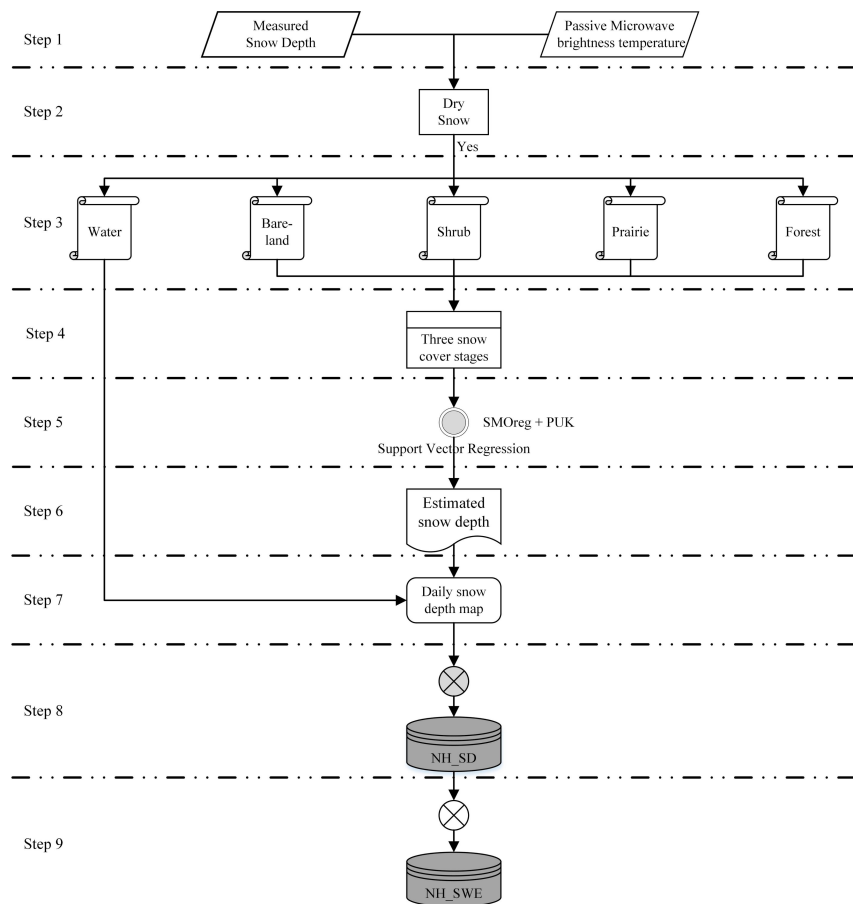
Figure 3. Process flowchart diagram for developing Northern Hemisphere daily snow depth and snow

water equivalent data
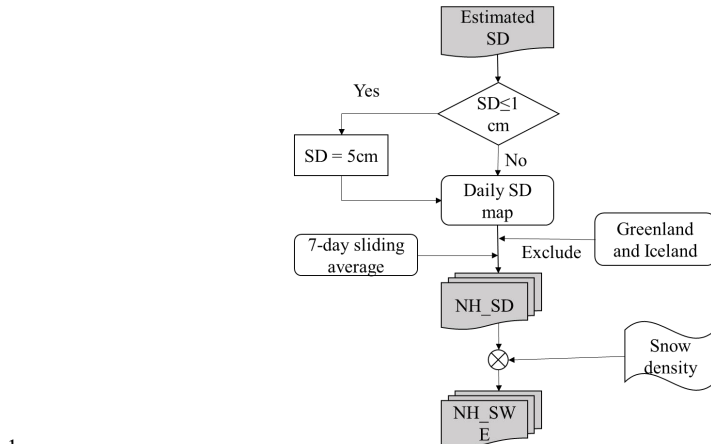
1

2   Figure 4. Flowchart diagram of the generation of NHSnow products.
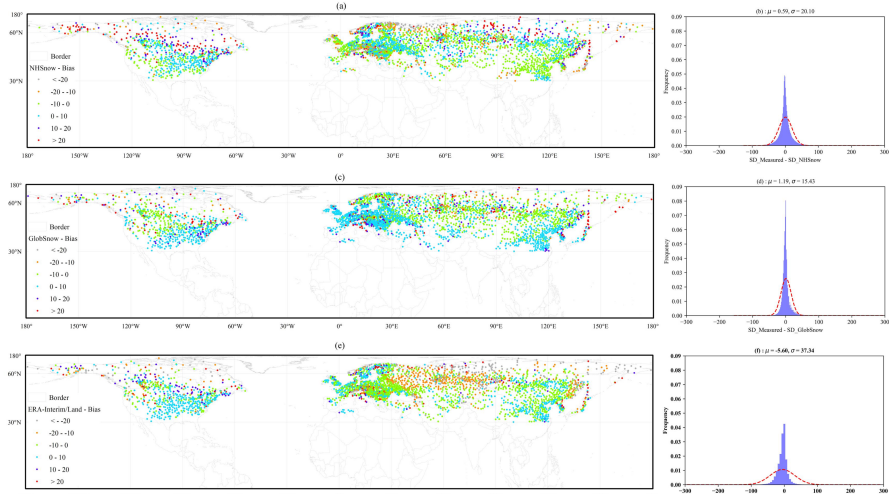
3

4   Figure 5. Bias of each meteorological station and histogram of biases for three products: a), b)

5   NHSnow; c), d) GlobSnow, e), f) ERA-Interim/Land. The red dashed line in right column figures are

6   the fitted normal distribution curve

7

34
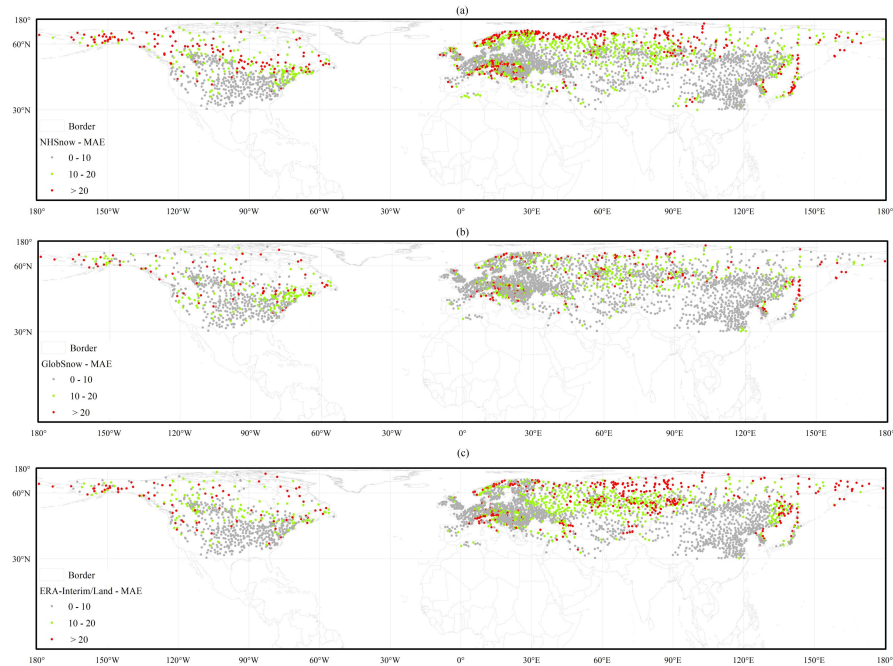
1

2   Figure 6. MAE of each meteorological station for three products: a) NHSnow, b) GlobSnow, c)
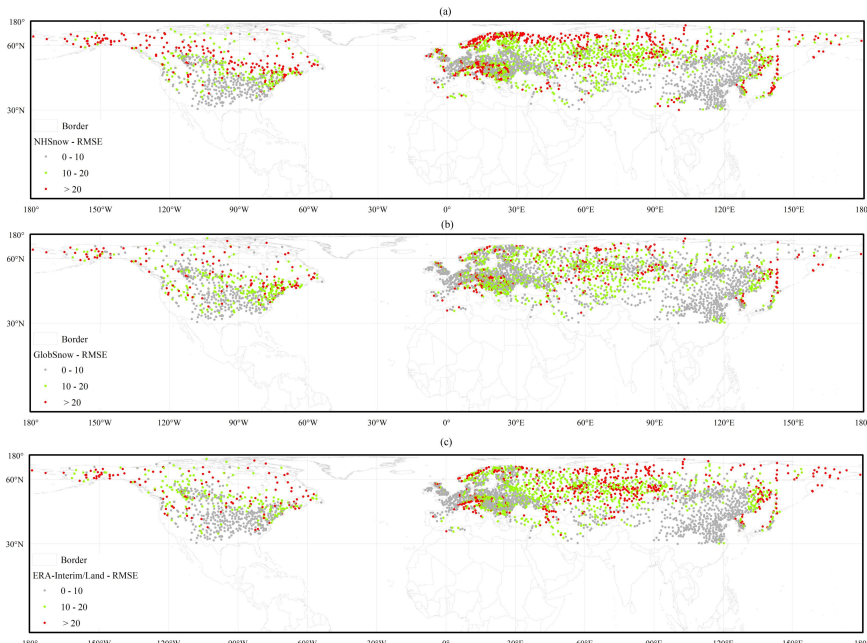
3   ERA-Interim/Land.


4

5   Figure 7. RMSE of each meteorological station for three products: a) NHSnow, b) GlobSnow, c)

35

1   ERA-Interim/Land.

2
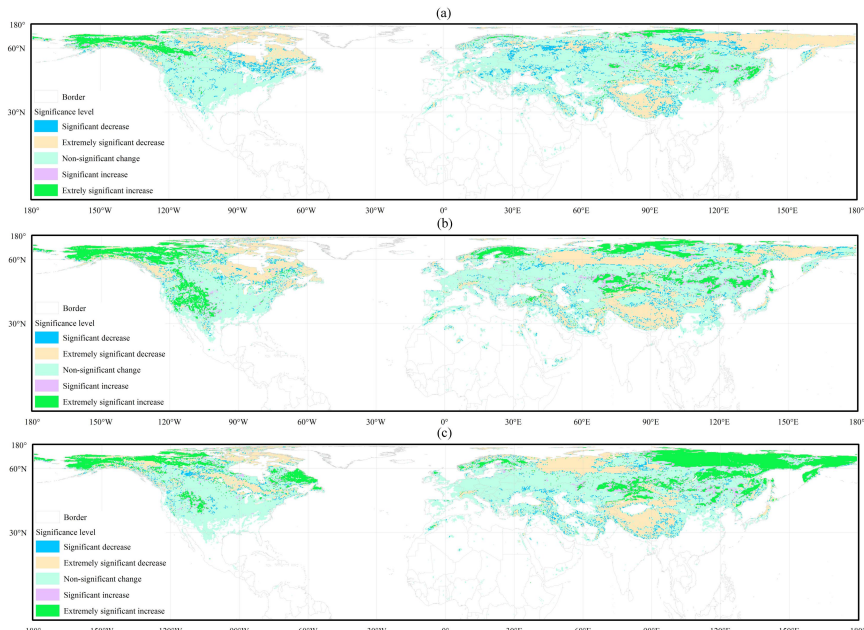
4   Figure 8. The variation rate pattern of season maximum SD with statistical significances over the

5   Northern Hemisphere for three snow cover season, fall (a; September to November), winter (b;

6   December to February), spring (c; March to June) from 1992-2016.
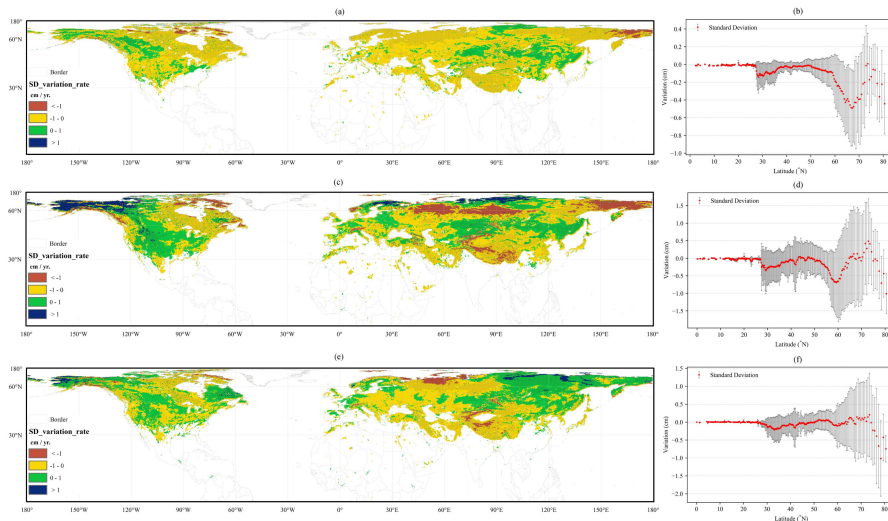
8   Figure 9. The variation rate pattern of season average SD over the Northern Hemisphere for three snow

1 cover season, fall (a, b; September to November), winter (c, d; December to February), spring (e, f;

2 March to June) from 1992-2016. Black dots in (a, c, e) indicate that the changes are significant at 95%

3 confidence level (CL). The zonal distribution in (b, d, f) are mapped at 0.25 degree resolution in

4 latitude. The error bars in (b, d, f) is one times of standard deviation.

5
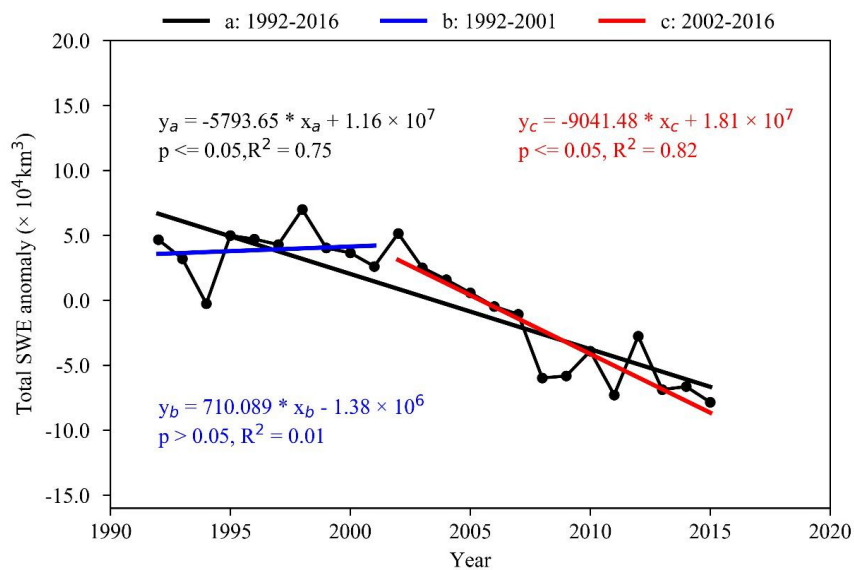
6

7 Figure 10. Interannual variation of total SWE over the Northern Hemisphere for three period

8 1992-2016 (black line), 1992-2001 (blue line), and 2002-2016 (red line), with respect to the 1992-2016

9 mean value. Trends estimates were computed from least squares. P is the confidence level for the

10 coefficient estimates, R^2 is the goodness of fit coefficient.
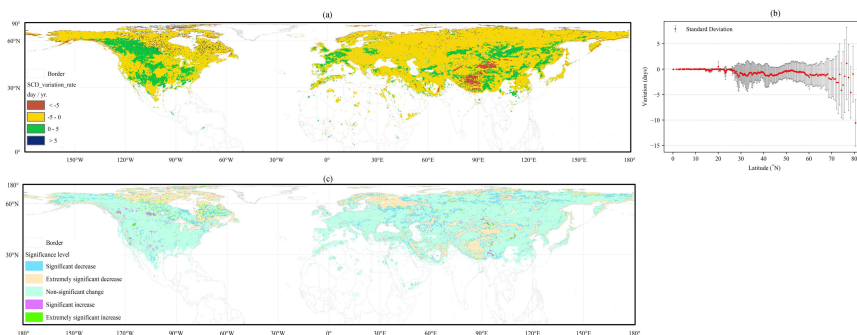
11

12 Figure 11. The variation rate pattern of SCD (a) and their statistical significances (c) over the Northern

1   Hemisphere from 1992-2016. The zonal distribution in (b) are mapped at 0.25 degree resolution in

2   latitude. The error bars in (b) is one times of standard deviation.

3